Versatile Regulation of Neuronal Nitric Oxide Synthase by Specific Regions of Its C-Terminal Tail†

Mauro Tiso,*,‡,§ Jesús Tejero,‡ Koustubh Panda,‡ Kulwant S. Aulak,‡ and Dennis J. Stuehr*,‡

Department of Pathobiology, Lerner Research Institute, Cleveland Clinic Foundation, Cleveland, Ohio 44195, and Department of Chemistry, Cleveland State University, Cleveland, Ohio 44115

Received August 14, 2007; Revised Manuscript Received September 18, 2007

ABSTRACT: The C-terminal tail (CT) of neuronal nitric oxide synthase (nNOS) is a regulatory element that suppresses nNOS activities in the absence of bound calmodulin (CaM). A crystal structure of the nNOS reductase domain (nNOSr) (Garcin, E. D., Bruns, C. M., Lloyd, S. J., Hosfield, D. J., Tiso, M., Gachhui, R., Stuehr, D. J., Tainer, J. A., and Getzoff, E. D. (2004) *J. Biol. Chem.* 279, 37918−37927) revealed how the first half of the CT interacts with nNOSr and thus provided a template for detailed studies. We generated truncation mutants in nNOS and nNOSr to test the importance of 3 different regions of the CT. Eliminating the terminal half of the CT (all residues from Ile1413 to Ser1429), which is invisible in the crystal structure, had almost no impact on $NADP^+$ release, flavin reduction, flavin autoxidation, heme reduction, reductase activity, or NO synthesis activity, but did prevent an increase in FMN shielding that normally occurs in response to NADPH binding. Additional removal of the CT α-helix (residues 1401 to 1412) significantly increased the $NADP^+$ release rate, flavin autoxidation, and NADPH oxidase activity, and caused hyper-deshielding of the FMN cofactor. These effects were associated with increased reductase activity and slightly diminished heme reduction and NO synthesis. Further removal of residues downstream from Gly1396 (a full CT truncation) amplified the aforementioned effects and in addition altered $NADP^+$ interaction with FAD, relieved the kinetic suppression on flavin reduction, and further diminished heme reduction and NO synthesis. Our results reveal that the CT exerts both multifaceted and regiospecific effects on catalytic activities and related behaviors, and thus provide new insights into mechanisms that regulate nNOS catalysis.

Nitric oxide (NO) is synthesized by the NO synthases (NOS; EC 1.14.13.39), a family of homodimeric flavo-heme enzymes that catalyze an NADPH-[1] and O_2-dependent oxidation of L-arginine (Arg) to L-citrulline and NO in a two-step process (*1*). Three distinct NOS isozymes, neuronal NOS (nNOS), inducible NOS (iNOS), and endothelial (eNOS), are expressed in mammals and have evolved to function in health and disease (*2*−*5*). Each NOS is composed of an N-terminal oxygenase domain that contains binding sites for iron protoporphyrin IX (heme), (6*R*)-tetrahydrobiopterin (H_4B) and Arg, and a C-terminal flavoprotein domain that contains binding sites for FAD, FMN, and NADPH (*6*, *7*). The two domains are linked by a central calmodulin (CaM) binding sequence. Ca^{2+}-dependent CaM binding triggers NO synthesis by enabling electron transfer from the FMN hydroquinone to the ferric heme. This enables the heme to bind O_2 and initiate its reductive activation as required for NO synthesis (*8*, *9*). The flavoprotein domain of NOS is structurally and functionally related to cytochrome P450 oxido-reductase (CYPOR) and related enzymes (*10*, *11*), and is composed of separate ferredoxin-$NADP^+$-reductase (FNR) and FMN modules (*12*, *13*). Protein constructs of the NOS flavoprotein domain with the attached CaM binding site (NOSr) have been used to study structural and regulatory aspects of NOS catalysis.

Electron transfer in NOSr and CYPOR starts with hydride transfer from NADPH to FAD within the FNR module, followed by electron transfer from the FAD hydroquinone to FMN (*14*−*16*). The reduced FMN module (containing FMN hydroquinone) must then swing away to transfer electrons to the NOS ferric heme or to unattached heme-protein acceptors like cytochrome *c* or the cytochrome P450's (*12*, *17*). Recent reports suggest that the steady-state activities of nNOSr and CYPOR are determined in part by regulation of a conformational equilibrium between the "FMN-shielded" or electron input state and the "FMN-deshielded" or electron output state of these proteins (*17*−*24*). What controls FMN shielding and how it relates to catalysis are topics of current interest. Bound NADP(H) stabilizes the FMN-shielded conformation in nNOSr (*19*, *21*) and CYPOR (*25*), implying

† This work was supported by National Institutes of Health Grants GM51491 and HL76491 to D.J.S. and by American Heart Association Fellowship 0415154B to M.T. and 0625632B to J.T.

* Address correspondence to these authors. Department of Pathobiology, NC-22, The Cleveland Clinic Foundation, 9500 Euclid Ave., Cleveland, OH 44195. Phone: (216)-445-6950. Fax: (216)-444-9329. E-mail: stuehrd@ccf.org & m_tiso@yahoo.com.

‡ Cleveland Clinic Foundation.

§ Cleveland State University.

[1] Abbreviations: nNOS, neuronal nitric oxide synthase; nNOSr, flavoprotein domain of neuronal nitric oxide synthase; wt, wild-type; CaM, calmodulin; FAD, flavin adenine dinucleotide; FMN, flavin mononucleotide; H_4B, (6*R*)-5,6,7,8-tetrahydro-L-biopterin; NADPH, reduced β-nicotinamide adenine dinucleotide; CT, C-terminal tail; AI, autoinhibitory insert; Pi, phosphate; EPPS, 4-(2-hydroxyethyl)-1-piperazinepropanesulfonic acid; DTT, dithiothreitol.

10.1021/bi701646k CCC: $37.00
Published on Web 11/20/2007

a similar regulation for these proteins. Nevertheless, the reductase activities of NOSr are suppressed relative to CYPOR and related flavoproteins, and CaM binding relieves the suppression (*26*), indicating that NOS has an additional, distinct regulation. Three unique structural elements appear to be involved in the catalytic suppression of NOS: an autoinhibitory element in the FMN binding module (*27*−*30*), a CD2A loop in the connecting subdomain (*31*), and a C-terminal extension or tail (CT, residues 1397−1429) (*32*−*37*). The recent crystal structure of nNOSr visualizes the first half of the CT, and shows how it interacts with nNOSr (*17*). The structure reveals that the CT may help stabilize the FMN-shielded conformation by holding the FMN module up against the FNR module as required for inter-flavin electron transfer. Indeed, the CT contains a central α-helix (residues 1401−1412) that interacts with the FMN module and provides a bonding network that may help shield FAD and FMN from solvent (*17*). Point mutagenesis done in this portion of the CT either to eliminate a charge pairing interaction between Arg1400 and the 2′-phosphate of bound NADPH (*21*) or to mimic phosphorylation at Ser1412 (*38*) partly relieved the suppression of nNOSr reductase activities. This further implicated the CT and suggested some molecular-level mechanisms of action (*17*, *21*).

On the basis of the above information, we generated truncation mutants that are missing increasing portions of the CT in both nNOS and nNOSr, to test the hypothesis that specific regions of the CT regulate different catalytic properties of nNOS. We studied 8 different aspects of each truncation mutant by conventional and stopped-flow spectroscopic methods. Our results define the relative contributions of each region of the CT and provide new understanding of how the CT and CaM regulate catalysis in nNOS.

EXPERIMENTAL PROCEDURES

Materials and General Methods. All reagents and materials were obtained from Sigma or sources previously reported (*39*, *40*). UV−visible spectra and steady-state kinetic data were recorded on a Shimadzu UV-2401PC spectrophotometer using quartz cuvettes. Single wavelength stopped-flow kinetic experiments were performed using a Hi-Tech (Salisbury, U.K.) SF-51MX instrument equipped for anaerobic work and photomultiplier detection (*41*). Full-spectra stopped-flow experiments were performed using a Hi-Tech SF-61 instrument equipped for anaerobic work and rapid-scanning diode array detection. The buffer used for all experiments and protein purifications (buffer A), unless noted otherwise, contained 40 mM EPPS (pH 7.6), 10% glycerol, and 150 mM NaCl. When necessary, samples were made anaerobic in an airtight cuvette by repeated cycles of vacuum followed by a positive pressure of catalyst-deoxygenated nitrogen. The nNOSr proteins were prepared for use by oxidizing the purified air-stable semiquinone form with potassium ferricyanide followed by passing the mixture through a PD-10 desalting column.

Molecular Biology. Restriction digestions, ligation, transformation, cloning, bacterial growth, and isolation of DNA fragments were performed using standard techniques. The selected C-terminal tail nNOS truncations were achieved by placing a stop codon at the appropriate position followed by an *Xba*I restriction site. nNOS cDNA fragments were PCR-generated using primers as follows: nNOS-tr1413 reverse primer is AAA ATCTAGA**TCA**GG ACT CAG ATC TAA GGC GGT; nNOS-tr1401 reverse primers is AAA ATCTAGA**TC** **A**TC TGA GGG TGA CTC CAA AGA, nNOS-tr1397 reverse primer is AAA ATCTAGA**TC** **A**TC CAA AGA TGT CCT CGT. Forward primer is in all cases GCT CAA CAG AAT ACA GGC TGA CG. Stop codon is denoted in bold, and *Xba*I sites are underlined. The PCR products were gel-purified and digested using *Xma*I (unique restriction site at nNOS cDNA position 3938) and *Xba*I (restriction site as designed) and ligated with purified *Xma*I−*Xba*I digested pCWori/nNOS cDNA reductase or full length. The resulting products were transformed to *Escherichia coli* XL10-gold competent cells (Stratagene), and positive colonies, selected with ampicillin, were identified by restriction digestion analysis. The sequences of mutations were confirmed at the Cleveland Clinic DNA sequencing facility. DNA containing the desired mutation was transformed into *E. coli* BL21 (DE3) cells for protein expression. Cells expressing nNOSr were also transformed with a pACYC plasmid containing human CaM and selected with chloramphenicol to coexpress CaM with the nNOSr protein.

Protein Expression and Purification. The wild-type and mutant rat nNOS and nNOSr proteins were overexpressed in *E. coli* strain BL21(DE3). The full-length nNOS proteins contained a His_6 tag in their N-termini to aid purification by a Ni-resin affinity column (*42*). The nNOSr proteins (construct 695−1429) were purified by sequential chromatography on a 2′,5′-ADP Sepharose affinity column and CaM-Sepharose resin as reported (*20*). The proteins were dialyzed against buffer A (see materials) and stored in aliquots at −80 °C. Purity of each protein was assessed by SDS−PAGE and spectral analysis. The concentration of the full-length nNOS proteins was estimated by quantification of heme protein content as evidenced through the formation of the ferrous−CO adduct with an absorption maximum at 444 nm (*43*). For the nNOSr proteins, concentration was determined by using an extinction coefficient of 22,900 M^{-1} cm^{-1} at 457 nm for the fully oxidized form (*14*).

Determination of Bound FAD and FMN. Bound flavins were released from a known amount of nNOS protein by heat denaturation of the enzyme for 3 min in the dark, followed by a short centrifugation. Flavin concentration in the supernatant was spectroscopically determined using an extinction coefficient of 12.2 mM^{-1} cm^{-1} at 447 nm. To determine the FAD/FMN ratio samples were injected onto a Cyano-18 HPLC column and flavins were detected by fluorescence emission following a published procedure (*44*).

NO Synthesis, NADPH Oxidation, and Cytochrome c Reduction. Steady-state activities were determined separately at room temperature using spectrophotometric assays as previously described (*44*). In order to compare with previously published data, in the case of NO synthesis and NADPH oxidation the assay buffer contained 150 mM NaCl while the assay buffer for cytochrome *c* reduction contained no added NaCl.

Interaction between the nNOSr Proteins and $NADP^+$. UV−visible spectral changes resulting from the association of $NADP^+$ with 20 μM nNOSr proteins were observed by calculating a difference spectrum between the fully oxidized protein before and after treatment with a 3-fold molar excess of $NADP^+$. For these experiments the nNOSr proteins were

first preincubated with 2′-AMP and then passed through a PD-10 desalting column prior to use in order to remove any $NADP^+$ that might remain bound to the proteins (*20*). The observed rate constant (k_{off}) values for the dissociation of $NADP^+$ from the oxidized nNOSr proteins were determined by rapidly mixing a solution containing nNOSr (60 μM) and $NADP^+$ (120 μM) with a solution of 2′,5′-ADP (4 mM) in the stopped-flow instrument at 10 °C and fitting the absorbance decreases at 510 nm to single-exponential functions using the software Origin 7.5 (OriginLab, Northampton, MA).

Autoxidation of Reduced nNOSr. A solution of nNOSr protein (3 or 5 μM) containing EDTA (0.5 mM) in air-saturated buffer was reduced by adding excess NADPH (100 μM) and then allowed to auto-oxidize at room temperature in an open cuvette. The process was monitored at 457 nm or visible spectra were recorded in replica experiments.

Anaerobic Stopped-Flow Flavin Reduction Kinetics. The absorbance changes associated with nNOSr flavin reduction by NADPH were recorded at 10 °C in the single-wavelength stopped-flow instrument by rapidly mixing a solution of oxidized nNOSr (6−8 μM) containing either EDTA (1 mM) or $CaCl_2$ (2 mM) + CaM (18−24 μM) with a solution of 60−100 μM NADPH. For each protein sample tested, the maximum absorbance value at 457 nm was obtained by replacing the NADPH solution in one of the stopped-flow syringes with anaerobic buffer and recording 2−3 additional mixing events. The individual rate constants were first estimated by analyzing experiments of different time duration. The final reported values were obtained by fitting to a quadruple exponential function experiments at a 2 s time scale, which enables estimation of four rate constants. The residuals were minimized and the signal-to-noise ratio was improved by averaging 4−5 individual mixing experiments. Percent absorbance changes were calculated for the absorbance change occurring in the instrument dead time (1.5 ms).

Anaerobic Pre-Steady-State Cytochrome c Reduction. A solution of each nNOSr protein (15−18 μM), glycine (3 mM), 5-deazariboflavin (≈1 μM), and either EDTA (1 mM) or $CaCl_2$ (2 mM) + CaM (30 μM) was completely photoreduced in an anaerobic cuvette using a commercial slide projector bulb until no changes in the UV−vis spectrum of the sample were observed upon further irradiation of the sample. The prereduced protein sample was rapidly mixed in the stopped-flow spectrophotometer with a solution of cytochrome *c* (3 μM) at 10 °C, and the absorbance change at 550 nm was recorded. In some cases 1 mM NADPH was added to the prereduced protein sample and the mixture was incubated at 10 °C for 15 min prior to mixing. Absorbance data were then fit to a single-exponential function using a nonlinear least-square method provided by the instrument manufacturer.

Heme Reduction Rate in Full-Length Proteins. Kinetics of heme reduction were analyzed at 10 °C using a stopped-flow spectrophotometer as described previously (*38*). Reactions were initiated by mixing an anaerobic, buffered, CO-saturated solution containing 10 μM NADPH with an anaerobic solution of 4 μM nNOS (wild type or mutant) in 100 mM EPPS pH 7.6, 150 mM NaCl, 10 μM H_4B, 0.4 mM DTT, 1 mM Arg, and 10 μM CaM. Heme reduction was followed by formation of the ferrous−CO complex at 444 nm. The time course of absorbance changes was fit to a single-exponential equation. An initial spectrum was recorded without NADPH to serve as a baseline. Signal-to-noise ratio was improved by averaging data from multiple individual mixing experiments.

Analysis of Stopped-Flow Data. In most cases, the spectral traces were fit according to single or multiple exponential equations. The best fit was designated when adding further exponentials did not improve the fit as judged by the residuals. In the case of flavin reduction by excess NADPH, we used a four exponential equation to fit the absorbance change at 457 nm, as done in previous reports (*20*, *21*, *45*).

Statistical Analysis. All experiments were repeated three or more times with at least two different batches of proteins purified separately. Data were analyzed and expressed as mean ± standard deviation of the mean. Analysis for statistically significant differences among mean values was done, when applicable, using Student's *t* test with a value of $p < 0.05$ considered as significant.

Modeling. The model for the nNOS reductase structure was produced by homology modeling through Swiss-Model (*46*, *47*) using the structure of nNOS reductase dimer (*17*) as template. All elements not visible in the crystal structure were modeled but the extension of the C-terminal tail (residues 1414−1429, rat nNOS numbering). This element was modeled separately using Swiss-Model and joined to the C-terminus of the nNOS structure (Ile 1413). The phi and psi angles for the linker residues (Ile 1413, Ala 1414) were manually adjusted. The geometry of the final structure was validated with PROCHECK (*48*) to verify that phi and psi values were in the allowed regions of the Ramachandran plot.

RESULTS

Mutant Protein Expression and Characterization. The CT truncations we generated in rat nNOS are illustrated in Figure 1. The tr1413 truncation removes only the portion of CT that is not visible in the crystal structure (1413−1429), while maintaining the α-helix and the phosphorylation-susceptible residue (Ser1412) that is known to be involved in determining CaM affinity and nNOS heme reduction rate (*38*). The tr1401 truncation additionally removes residues that create the CT α-helix but preserves the critical residue Arg1400 which makes a charge pairing interaction with the 2′Pi of bound NADPH (*17*). The tr1397 truncation additionally removes 4 residues (1397−1400) at the start of the CT that make hydrophobic contacts (Val1397−Ala888), hydrogen bonds (Val1397−Tyr889, Thr1398/Leu1399−Asp1351) or ionic interactions (Arg1400) with the FMN or FNR modules. The tr1397 truncation compromises the entire CT (all residues downstream from Gly1396) and is equivalent to the nNOS-tr1 previously studied by Roman et al. (*32*). The tr1413, tr1401, and tr1397 mutants were expressed both as the nNOSr and full-length nNOS enzyme constructs. In general the nNOSr enzymes were obtained in greater yield (about 15−20 mg/L) than the full-length proteins (6−10 mg/L). Flavin analysis showed that all nNOS proteins incorporated 2 mol of flavin (FAD + FMN) per subunit (data not shown). Spectrophotometric analysis of the full-length proteins showed that H_4B and Arg binding caused their heme Soret bands to shift to a high-spin state, and reduction of the

FIGURE 1: Protein constructs used in the study. The C-terminal of rat nNOS contains a highly conserved region (RYHEDIFG, bold) that precedes the CT. The composition of the nNOS wild-type and truncation mutants are shown. CT residues Arg1400 and Ser1412 are in bold.

Table 1: Apparent k_{cat} Values for Cytochrome *c* Reductase Activities Supported by NADPH in nNOS Wild-Type and Truncation Mutants[a]

nNOS reductase			nNOS full-length		
enzyme	−CaM (min^{-1})	+CaM (min^{-1})	enzyme	−CaM (min^{-1})	+CaM (min^{-1})
wt	430 ± 81	4272 ± 191	wt	463 ± 78	5320 ± 243
tr1413	683 ± 109	3413 ± 340	tr1413	495 ± 54	5817 ± 520
tr1401	2049 ± 162	3325 ± 260	tr1401	3088 ± 237	6264 ± 274
tr1397	3121 ± 196	3461 ± 386	tr1397	6402 ± 306	3580 ± 371

[a] The apparent k_{cat} values were calculated from cytochrome *c* reductase activities determined at 25 °C as described in Experimental Procedures. Values are the mean ± SD from triplicate experiments representative of two independent enzyme preparations and are expressed as mole of product formed per mole of enzyme per min.

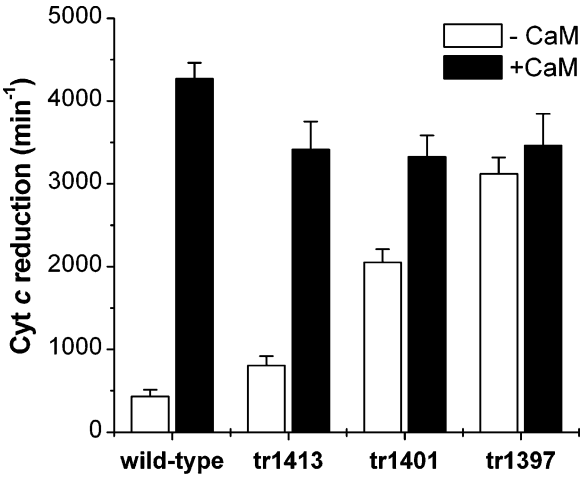

FIGURE 2: Cytochrome *c* reductase activity of wild-type and CT truncation mutants of nNOSr. The reactions were run at room temperature as described in Experimental Procedures. Each experiment was performed in triplicate, and values are representative of two or more independent determinations.

enzymes in the presence of CO produced the expected 444 nm Soret absorbance peak for the ferrous heme−thiolate CO complex (data not shown). These findings indicate that CT truncation does not grossly perturb NOS structure, prosthetic group and substrate binding, or heme electronic environment, consistent with previous results (*32*, *33*, *35*).

Cytochrome c Reductase Activity. The steady-state cytochrome *c* reductase activity of nNOS can quantify the electron flux through its reductase domain. Table 1 contains apparent k_{cat} values for cytochrome *c* reductase activities supported by NADPH in the nNOSr and full-length nNOS wt and CT truncation mutants. In the absence of Ca^{2+}/CaM, the increasing severity of CT deletion resulted in increased cytochrome *c* reduction as shown in Figure 2. Compared to the nNOSr wt, the nNOSr tr1413 displays less than a 2-fold increase in reductase activity, while the tr1401 and tr1397 activities are respectively 5- and 8-fold greater. In the presence of Ca^{2+}/CaM the cytochrome *c* reductase activity was comparable with wild-type enzyme in all the nNOSr truncations mutants, however their absolute values were 10% to 20% lower. The full-length nNOS CT truncated enzymes, in the absence of CaM, exhibited a similar response to increasing CT deletion with the largest increase in rate observed for nNOS tr1397 (14-fold increase). The data indicate that CT residues beyond Ser1412 (1413−1429) do not play a major role in suppressing activity toward external electron acceptors like cytochrome *c* in CaM-free nNOS. On the other hand, the remaining residues of the CT show a graded degree of importance, and both the α-helix and four residues immediately upstream from it (1397−1400) are necessary for suppression in the absence of CaM. A comparison of cytochrome *c* reductase activities between the mutant reductase and full-length enzymes (Table 1) revealed significant ($p < 0.05$) differences in their absolute values. In particular, the activities of the CaM-bound full-length nNOS tr1413 and tr1401 mutants were on average 2-fold higher than the respective nNOSr enzymes. However, the full-length nNOS tr1397 showed a 2-fold increase only in the CaM-free condition. Also, binding CaM inhibited its cytochrome *c* reduction activity as previously reported (*32*). These results suggest that CT control of NOS reductase activity is not always equivalent in the full-length nNOS and the nNOSr.

Interactions of nNOSr enzymes with NADP$^+$. Because the CT is located near the site of NADPH binding in nNOSr (*17*), we investigated if the CT deletions would alter enzyme interactions with bound $NADP^+$. It has been reported (*49*−*51*) that the nicotinamide ring of $NADP^+$ can engage in an aromatic stacking interaction with the FAD isoalloxazine ring of CYPOR and NOS. This interaction shifts the flavin absorbance spectrum in a characteristic manner. Typically, analysis by difference spectroscopy reveals an absorbance increase centered near 510 nm that correlates with the degree of nicotinamide−FAD stacking (*52*−*54*). We investigated this interaction in the nNOSr truncation mutants (in their fully oxidized state) by monitoring changes in their visible absorption spectrum upon $NADP^+$ addition (Figure 3 inset). Compared to nNOSr wt, binding of $NADP^+$ in the nNOSr tr1413 and tr1401 caused a smaller 510 nm difference absorption peak and caused no observable absorption change in the nNOSr tr1397. The data suggest that, when CT is partially truncated, the nNOSr can still engage in a normal nicotinamide−FAD stacking interaction, but to a lesser extent than in nNOSr wt. The full CT truncation does not allow a normal interaction with $NADP^+$, at least when FAD is in the fully oxidized state. We can estimate the extent of the nicotinamide−FAD stacking interaction in wild-type nNOSr and each truncation mutant by comparing their 510 nm difference absorption values to that obtained for the F1395S nNOSr mutant, which supports the maximum (arbitrarily assigned as 100%) stacking interaction between FAD and $NADP^+$ (*20*). This calculation indicates a nicotinamide−FAD stacking of 34%, 20%, and 15% in the wild-type, tr1413, and tr1401 nNOSr proteins, respectively.

As previously shown (*20*), mixing the $NADP^+$-bound nNOSr with an excess of 2′,5′-ADP results in a time-dependent absorbance decrease at 510 nm which can be used

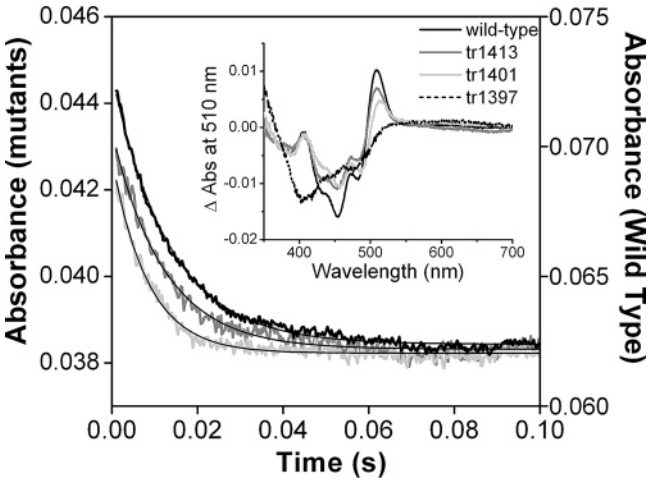

FIGURE 3: Kinetics of $NADP^+$ dissociation. $NADP^+$-saturated nNOSr proteins were rapidly mixed with an excess of 2′,5′-ADP in the stopped-flow instrument at 10 °C as described in Experimental Procedures. The absorbance decreases at 510 nm are shown along with the calculated lines of best fit. Inset: Difference spectra elicited by the binding of $NADP^+$ to each nNOSr protein.

Table 2: Kinetics of $NADP^+$ Dissociation from Wild-Type nNOSr and Truncation Mutants[a]

nNOSr enzyme	rate of $NADP^+$ dissociation (k_{off}) (s^{-1})	total abs change (mOD)	% nicotinamide occupancy
wild-type	75 ± 0.1 (33%)	15	34
tr1413	82 ± 0.1 (50%)	9	20
tr1401	119 ± 0.2 (49%)	7	15
tr1397	nd	nd	0

[a] Enzyme samples containing bound $NADP^+$ were mixed at 10 °C in a stopped-flow spectrophotometer with an excess of 2′,5′-ADP, and the absorbance decrease at 510 nm was recorded as described in Experimental Procedures. The curves were fit to single-exponential decay function yielding the observed k_{off} rates. The number in parentheses indicates the percentage of absorbance change occurring in the instrument mixing dead time. The values are the mean ± SD of 5−6 single mixing experiments and are representative of 2 different enzyme preparations each; nd, not detected.

to estimate the dissociation rate of $NADP^+$ from the enzyme. A concentration of 4 mM 2′,5′-ADP was used to minimize rebinding of the released $NADP^+$ from 30 μM $NADP^+$-saturated nNOSr protein (Figure 3, main panel). The traces of absorbance were fit to a single-exponential decay function to yield the observed $NADP^+$ dissociation rate (k_{off}) at 10 °C. Rates are reported in Table 2 along with the total absorbance change measured for each protein. The k_{off} values for $NADP^+$ dissociation were faster for nNOSr tr1413 and tr1401 than in nNOS wt by 1.1- and 1.5-fold, respectively. The numbers in parentheses indicate the percentage of absorbance change occurring during the instrument dead time (about 1.5 ms). It was found that in the CT truncated proteins about half of the total absorbance change occurs in the instrument dead time compared to 1/3 for the nNOSr wt. Thus, the α-helix and upstream portion of the CT impacts $NADP^+$ binding in nNOS by enabling a nicotinamide−FAD interaction and by decreasing the release rate of $NADP^+$.

Kinetics of Flavin Reduction by NADPH. The rate of NADPH-dependent flavin reduction is suppressed in CaM-free nNOSr, and the suppression is relieved upon CaM binding (*20*, *55*). To see if the CT is involved in this process, we measured rates of NADPH-dependent flavin reduction

Table 3: Kinetic Analysis of NADPH-Dependent Flavin Reduction in the nNOSr Enzymes[a]

nNOSr	condition	k_1 (s^{-1})	k_2 (s^{-1})	k_3 (s^{-1})	k_4 (s^{-1})
wild-type	−CaM	64 ± 5	6.7 ± 2	2.2 ± 0.9	0.009 ± 0.008
	+CaM	160 ± 36	12 ± 2	2.6 ± 1.1	0.016 ± 0.006
tr1413	−CaM	77 ± 2	6.8 ± 0.3	2.1 ± 0.1	0.054 ± 0.013
	+CaM	112 ± 4	16 ± 0.8	4.1 ± 0.1	0.140 ± 0.002
tr1401	−CaM	76 ± 2	11 ± 0.7	2.5 ± 0.1	0.074 ± 0.004
	+CaM	103 ± 5	16 ± 1	3.3 ± 0.1	0.110 ± 0.009
tr1397	−CaM	128 ± 8	17 ± 1	1.9 ± 0.2	0.061 ± 0.004
	+CaM	116 ± 5	15 ± 1	2.0 ± 0.1	0.072 ± 0.002

[a] Reactions were initiated by mixing each oxidized enzyme with a 10-fold excess of NADPH under anaerobic conditions in a stopped-flow instrument at 10 °C. The absorbance change at 457 nm was fit to a quadruple exponential function. The percentage of the total absorbance change occurring in the instrument mixing dead time was between 24% and 30% for all the proteins tested.

in all mutants in the presence or absence of CaM. The stopped-flow traces fit well to a quadruple exponential function, and thus four rate constants were obtained following a previously described analysis for nNOSr (*20*, *21*, *45*). Data are summarized in Table 3. For each experiment, an initial absorbance value representing no flavin reduction was also obtained. In all cases a significant amount of the total absorbance change took place in the dead time of the instrument, consistent with previous reports for nNOSr (*19*−*21*, *56*). The kinetics of flavin reduction in the CaM-free nNOSr tr1413 and tr1401 mutants was analogous to the nNOSr wt. However, the CaM-free nNOSr tr1397 had considerably faster flavin reduction and was similar to the CaM-bound wild-type nNOSr. Binding CaM to tr1397 caused no further increase in the rate of flavin reduction. Our data show that the four residues upstream from the CT α-helix are required to suppress the rate of flavin reduction in CaM-free nNOSr.

Pre-Steady-State Cytochrome c Reduction. To determine how the CT may regulate FMN shielding in nNOS, we utilized an established stopped-flow spectroscopic method (*19*−*21*) to measure the rate of electron transfer to cytochrome *c* by each photoreduced nNOSr protein under three different conditions: as is, plus NADPH, and plus NADPH and CaM. Each absorbance trace fit well to a monoexponential curve, and the rate values we obtained for the nNOSr enzymes are reported in Table 4 and compared in Figure 4. The observed rate under the basal (NADPH- and CaM-free) condition was similar in wt and the tr1413 mutant, but was 4 to 5 times faster in tr1401 and tr1397 mutants. This reveals that the CT α-helix helps to determine the set point for FMN shielding in nNOS. NADPH binding to CaM-free wt nNOSr caused a 4-fold rate decrease, consistent with previous results showing that bound NADPH stabilizes the FMN-shielded conformation of nNOSr (*19*−*21*). In contrast, NADPH binding caused no decrease in rate for the tr1413, tr1401, and tr1397 mutants. This reveals that the terminal half of the CT is required for NADPH to increase FMN shielding in CaM-free nNOSr. When CaM bound to the NADPH-bound mutant enzymes we observed a rate increase in tr1413 nNOSr but saw little or no increase in the tr1401 and tr1397 mutants. Thus, CaM can no longer alter FMN shielding in the absence of the CT α-helix.

Flavin Autoxidation. Full truncation of CT was reported to increase the rate of flavin autoxidation in nNOS (*32*). To

Table 4: Effect of CaM and NADPH on the Rate of Electron Transfer to Cytochrome *c* by Prereduced nNOSr and the Truncation Mutant Enzymes[a]

nNOSr enzyme	observed rate (s^{-1}) −CaM −NADPH	−CaM +NADPH	+CaM +NADPH
wild-type	23 ± 1.2	5.8 ± 0.5	41 ± 0.5
Tr1413	23 ± 0.6	24 ± 0.4	46 ± 0.6
Tr1401	92 ± 2.2	96 ± 3.4	102 ± 4.2
Tr1397	111 ± 6.7	102 ± 1.5	148 ± 2.4

[a] An excess of each prereduced nNOSr protein in the presence or absence of NADPH and CaM was mixed with cytochrome *c* in a stopped-flow spectrophotometer under anaerobic conditions at 10 °C as described in Experimental Procedures. The observed rates of absorbance increase at 550 nm are reported as the mean ± SD of 5−6 single mixing experiments and are representative of at least 2 different enzyme preparations.

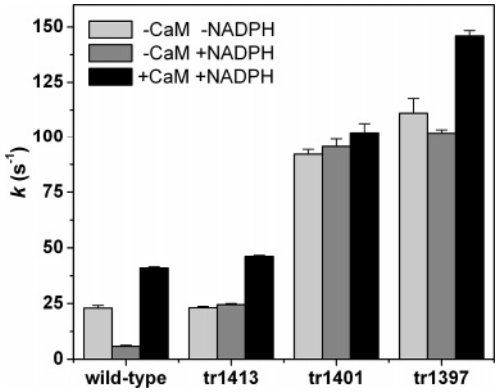

FIGURE 4: Rates of cytochrome *c* reduction by photoreduced nNOSr proteins under various conditions. The observed rates that were obtained in pre-steady-state cytochrome *c* reduction experiments as reported in Table 5 are plotted for each nNOSr protein to indicate the effects of NADPH and CaM binding on the rate of electron transfer to cytochrome *c*. The bars indicate the mean rate ± SD.

compare how the different CT truncations affect flavin oxygen reactivity, we added 100 μM NADPH to each fully oxidized nNOSr enzyme in air-saturated buffer, and then monitored the time required for each enzyme to consume the NADPH and then reoxidize. Flavin absorbance traces monitored at 457 nm are shown in Figure 5. The nNOSr tr1413, tr1401, and tr1397 mutants consumed the NADPH approximately 1.5, 4, and 5 times faster than did nNOSr wt, respectively. After the NADPH was oxidized, the subsequent absorbance gains indicated that reduced flavins in the mutants reoxidized 3 to 5 times faster compared to wt. The final absorbance values at 457 nm were similar in all three enzymes, indicating that they each reoxidized to a fairly stable one-electron-reduced state that presumably contains the FMN semiquinone radical (*57*, *58*). Thus, the O_2 reactivity of the reduced flavin species increased with the extent of CT deletion, and the greatest increase in reactivity was obtained upon deletion of the CT α-helix.

NO Synthesis and NADPH Oxidation Activities. We utilized full-length nNOS enzymes to investigate how the CT truncations would affect NO synthesis and NADPH oxidation activities, and the values are listed in Table 5. In the absence of CaM the nNOS wild-type, tr1413, and tr1401 truncation mutants had no detectable NO synthesis, as judged by the oxyhemoglobin assay (data not shown, the assay detection limit in our conditions is 0.5 min^{-1}). However, the

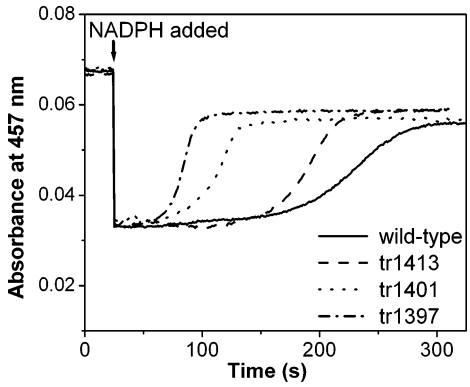

FIGURE 5: Kinetics of NADPH consumption and flavin autoxidation by the nNOSr proteins. The nNOSr proteins were diluted to 3 μM in air-saturated buffer in a cuvette, given 100 μM NADPH, and then allowed to consume NADPH at room temperature as described under Experimental Procedures. Data are representative of three independent experiments.

Table 5: Steady-State NO Synthesis Activities and Associated NADPH Oxidation Rate for nNOS and the Truncation Mutants[a]

nNOS enzyme	NADPH oxidation during Arg reaction (min^{-1}) −CaM	+CaM	NO synthesis from Arg (min^{-1}) −CaM	+CaM
wild-type	3.0 ± 1.1	107 ± 8.8	nd	53 ± 4
tr1413	5.6 ± 1.2	119 ± 16	nd	49 ± 5
tr1401	53 ± 4.9	138 ± 15	nd	40 ± 2
tr1397	83 ± 3.9	185 ± 15	3.0 ± 0.5	27 ± 2

[a] Rates of NO synthesis and NADPH oxidation are expressed as moles of product per mole of heme per min and were derived from assays run at room temperature as described in Experimental Procedures. The values are the mean ± SD of three separate measurements, two enzyme preparations each; nd, not detectable.

nNOS tr1397 displayed a low but detectable NO synthesis activity (3 min^{-1}), as previously reported (*32*). Using *N*-hydroxy-L-arginine in place of Arg as a substrate for the NO synthesis reaction did not change these results (data not shown). In the presence of CaM the nNOS tr1413, tr1401, and tr1397 mutants had 10%, 20%, and 45% lower NO synthesis rates, respectively, compared to nNOS wild-type (rank order was wild-type > tr1413> tr1401> tr1397). This suggests that the CT truncations have a relatively mild effect on NO synthesis activity until a full CT deletion is achieved.

The rates of NADPH oxidation increased in the CT-truncated enzymes. Compared to the CaM-free wild-type nNOS, the tr1413, tr1401, and tr1397 nNOS enzymes increased respectively by 2-, 18-, and 27-fold. Thus, the greatest increases were seen when the CT α-helix had been deleted (tr1401 and tr1397), consistent with the analogous nNOSr mutants having similarly increased rates of flavin autoxidation (Figure 5). NADPH oxidation by the CaM-bound tr1413, tr1401, and tr1397 nNOS mutants also increased during their NO synthesis by 1.1-, 1.4-, and 1.8-fold over wild-type nNOS, respectively. In this circumstance the differences between the values measured for the mutant and the wild-type enzymes could be accounted for by their increased rates of NADPH oxidation seen under the CaM-free condition. This indicates that CaM binding did not significantly alter the uncoupled NADPH consumption associated with the truncations. The ratio between NADPH consumption and NO synthesis from Arg in CaM-bound, wild-type nNOS was 1.9, but this ratio increased to about 3

Table 6: Kinetics of Heme Reduction in Wild-Type nNOS and Mutants[a]

nNOS enzyme	rates of ferric heme reduction (s^{-1})
wild-type	4.3 ± 0.4
Tr1413	4.1 ± 0.3
Tr1401	3.6 ± 0.4
Tr1397	1.9 ± 0.5

[a] Solutions of CaM-bound nNOS enzymes were mixed at 10 °C with excess NADPH under a CO atmosphere in the stopped-flow spectrophotometer, and the rate of ferrous−CO complex formation was determined at 444 nm. The observed rates are the mean ± SD from 5 to 6 runs and representative of 3 to 4 independent measurements using two enzyme preparations.

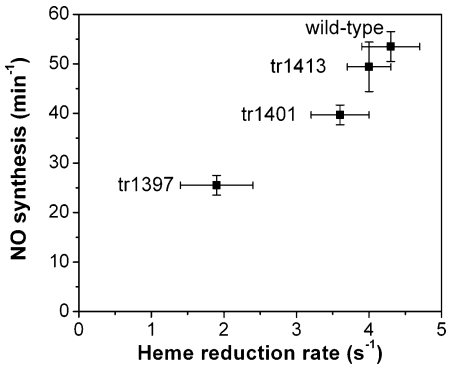

FIGURE 6: Relationship between the steady-state NO synthesis activity and the ferric heme reduction rate in the full-length nNOS proteins. Points are the mean values ± SD for the NO synthesis activities and heme reduction rates listed in Tables 5 and 6.

in tr1401 and to 6 in tr1397. The increase in uncoupled NADPH oxidation was associated with a lower NO synthesis activity in the tr1401 and tr1397 mutants.

Anaerobic Rate of Heme Reduction. We measured rates of ferric heme reduction in the CaM-bound nNOS enzymes to determine if their lower NO synthesis activities were associated with slower rates of heme reduction. Heme reduction was monitored by following the formation of the ferrous heme−CO complex at 444 nm after mixing each CaM-bound enzyme with excess NADPH under anaerobic conditions in a stopped-flow spectrophotometer (*21*, *38*). Ferric heme reduction was monophasic in all the enzymes, and the observed rates of heme reduction are listed in Table 6. The tr1413 and tr1401 mutants had rates of heme reduction that were slightly lower than in wild-type nNOS, while the tr1397 mutant had a rate that was about 50% slower. A plot of the NO synthesis activities versus the heme reduction rates indicates that a direct relationship exists between the two parameters in the CT-truncated enzymes (Figure 6).

DISCUSSION

Our previous crystallographic and mutagenesis studies (*17*, *21*, *38*) guided the design of partial CT truncations to further dissect its function in nNOS. The current results reveal new roles for CT in regulating NADPH binding, flavin reduction rate, FMN shielding, and heme reduction in nNOS, and show how three regions of the CT impact each of these aspects in relation to catalysis. It is known that electron import and export are suppressed in CaM-free nNOSr (*55*, *57*), that its FMN module is relatively shielded from solvent (*19*, *20*, *22*, *57*), and that CaM binding relieves the suppression of these parameters. Table 7 summarizes how each of the 3 CT truncations affected these and other parameters compared to CaM binding to nNOS. In general, the CT truncations mimicked, and in some cases exceeded, the changes caused by CaM binding. As truncation of the CT grew more extensive, a greater number of parameters were affected, some to a graded extent. The details are discussed below in the context of the CT and nNOS structure−function.

Wild-Type versus tr1413. Remarkably, results with the tr1413 mutants show that the entire terminal half of CT has almost no role in suppressing catalysis, the rate of flavin reduction, or protecting against flavin autoxidation in CaM-free nNOSr. This means that the first half of the CT, which is the portion that is visible in the nNOSr crystal structure (*17*), is practically functional on its own. To better comprehend this finding, we modeled the terminal half of CT, and then attached one of its probable structures to the existing structure of nNOSr (Figure 7A). In this representation the terminal half of CT forms a helix that can extend over the surface of the FMN module. Although this is only one of several protein conformations with similar energy, it serves to illustrate the scope of the tr1413 truncation. Moreover, placement over the FMN module is consistent with the terminal half of CT helping to control the conformational equilibrium of the FMN module. This role is demonstrated by our finding that NADPH no longer increases FMN shielding in tr1413 nNOSr, whereas it causes about a 4-fold increase in FMN shielding in wild-type nNOSr (Table 7). The crystal structure of nNOSr shows that Arg1400 in the first half of CT contacts bound NADPH, and mutagenesis of this residue can also prevent the NADPH-induced increase in FMN shielding (*21*). Perhaps this interaction with NADPH directs *both* the CT α-helix and the terminal half of CT to stabilize the FMN module in the shielded conformation (Figure 7A). This possibility can now be investigated.

Even though NADPH could no longer increase FMN shielding in tr1413 nNOSr, its cytochrome *c* reductase activity was only 1.6 times greater than that of the wild-type CaM-free nNOSr (Table 1). This result is surprising, because the NADPH-induced increase in FMN shielding has been assumed to be the major contributing factor in suppressing the reductase activity of CaM-free nNOSr relative to the CaM-bound enzyme (*19*, *21*). As our current data suggest, this may not be the case; further work is needed to clarify the discrepancy and/or identify the factors that suppress catalysis in CaM-free nNOSr.

Tr1413 versus tr1401. Additional truncation of CT to delete its α-helix greatly increased all the measured parameters reported in Table 7 except for the flavin reduction kinetics. Clearly, the α-helix is essential and it appears to be the central structural feature that enables the CT to suppress CaM-free nNOS. Deleting the CT α-helix also greatly influenced the FMN shielding equilibrium. Indeed, our data indicate that the FMN in CaM-free tr1401 is twice less shielded than in CaM-bound nNOSr, and therefore exists in a "hyper-deshielded" state. This drop in FMN shielding was associated with a 5-fold increase in cytochrome *c* reductase activity, consistent with an inverse relationship between FMN shielding and the reductase activity of CaM-free nNOSr (*19*, *20*). This concept is further discussed in a later paragraph.

Deleting the CT α-helix greatly increased the NADPH oxidase activity and flavin autoxidation rate of nNOSr. These

Table 7: Comparative Effects of the CT Truncations[a]

nNOSr − CaM	wild-type	tr1413	tr1401	tr1397	wild-type + CaM
Cyt *c* reductase activity	1	1.6	5	8	9
NADPH oxidation activity	1	2	18	27	2.5 (*57*)
k_{off} $NADP^+$	1	1.1	1.6	nd	1 (*20*)
flavin autoxidation rate	1	1.5	4	5	1.5
flavin reduction rate (k_1)	1	1.2	1.2	2	2.5
flavin reduction rate (k_2)	1	1	1.7	2.5	1.8
relative level of FMN deshielding[b]	1	1	4	4.8	2
effect of NADPH on FMN deshielding[c]	0.25	1.1	1.1	0.9	1.3 (*21*)

nNOS + CaM	wild type	tr1413	tr1401	tr1397
NO synthesis activity	1	0.9	0.8	0.5
heme reduction rate	1	1	0.8	0.4

[a] The numbers are the mutant to wild-type ratio and were calculated using values reported in this manuscript or in the references noted in parentheses; nd, not detectable. [b] In the NADPH-free condition. [c] Ratios are calculated relative to the value obtained for each CaM-free protein in the absence of NADPH.

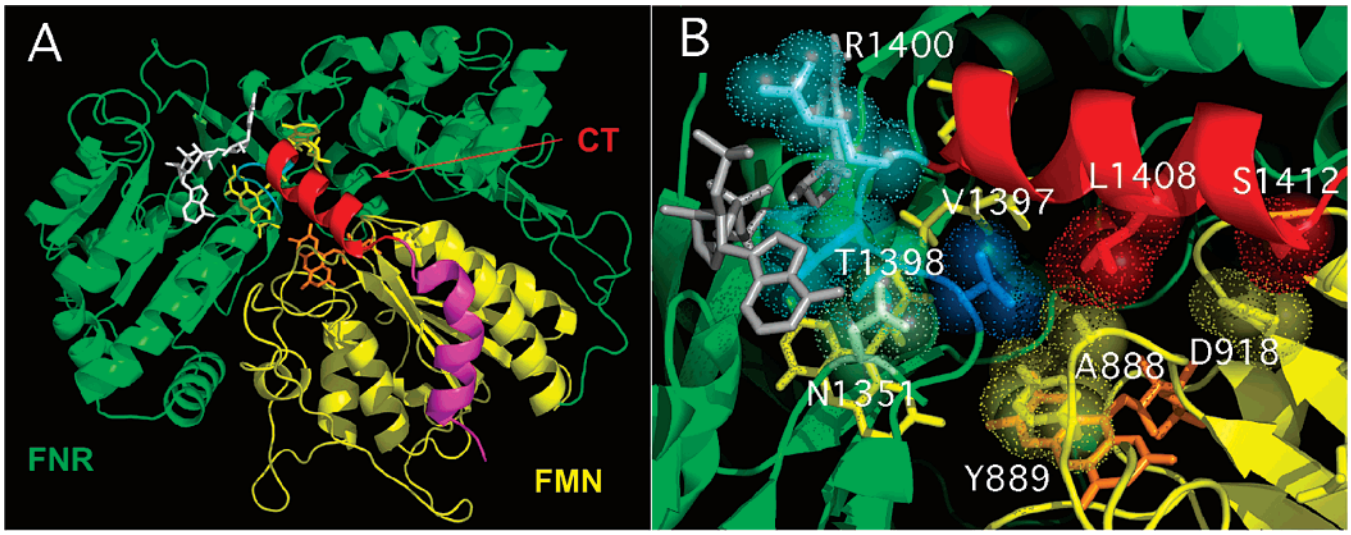

FIGURE 7: Panel A. The nNOSr structure featuring interactions of the CT. The FMN binding domain is yellow, and the remaining subdomains of nNOSr are green. The bound cofactors NADPH, FAD, and FMN are shown in white, yellow, and orange, respectively. The CT (residues 1397−1429) is color-coded to correspond with the tr1413, tr1401, and tr1397 truncations: the portion of CT not visible in the nNOSr crystal structure 1TLL (residues 1413−1429, modeled here as a magenta helix); the CT α-helix (residues 1401−1412, red); the upstream CT residues (1397−1400, cyan). Panel B. Interactions between CT residues and residues or cofactors located in other nNOSr subdomains. Coloring is according to panel A. See text for details.

two effects are linked and underscore the importance of the CT α-helix in limiting O_2 reaction with the reduced flavins in nNOS. Although the protective mechanism is unclear, the CT α-helix may restrict O_2 access to the flavins by covering part of the subdomain interface (*17*, *32*). Alternatively, it could restrict the conformational freedom of the FMN module or coordinate its movement to the redox state of the FAD and FMN cofactors. In any case, it is remarkable that nNOS evolved to rely on CT for this protection, because all flavoproteins related to NOS have no CT and must minimize their flavin autoxidation by other means. The changes we observed in tr1401 nNOSr are consistent with the CT α-helix making numerous contacts with the FNR and FMN modules as evident in the nNOSr crystal structure (*17*). These include the hydrophobic contacts, hydrogen bonds, and ionic interactions shown in Figure 7B that appear to provide a bonding network that helps the CT protect the flavins and stabilize the FMN-shielded conformation.

Tr1401 versus tr1397. The tr1397 truncation eliminates the entire CT and is equivalent to the nNOS-tr1 previously studied by Roman et al. (*32*). In our hands, additional deletion of the four CT residues upstream from the α-helix caused most parameters in Table 7 to increase by a moderate degree. The cytochrome *c* reductase activity and flavin reduction rate almost doubled to become nearly equivalent to those measured for CaM-bound nNOSr. In addition, the NADPH−nicotinamide−FAD interaction was further altered, there was a greater deshielding of the FMN module, there was a greater flavin autoxidation, and this was the only truncation that relieved the kinetic suppression on flavin reduction. Together, this shows that the full CT deletion completely relieved suppression of nNOSr, but also caused some changes that are not observed in the shorter CT truncations or upon CaM binding. The crystal structure indicates that deletion of the four residues 1397−1400 will remove hydrophobic contacts (Val1397−Ala888), hydrogen bonds (Val1397−Tyr889, Thr1398/Leu1399−Asp1351), and ionic interactions (Arg1400−2′Pi of NADPH) made between CT and the FMN or FNR modules in nNOSr (Figure 7B). Our results imply that these contacts enable some suppression even without the rest of the CT. The four residues also provide protection against flavin autoxidation and enable a normal NADPH binding interaction in nNOSr.

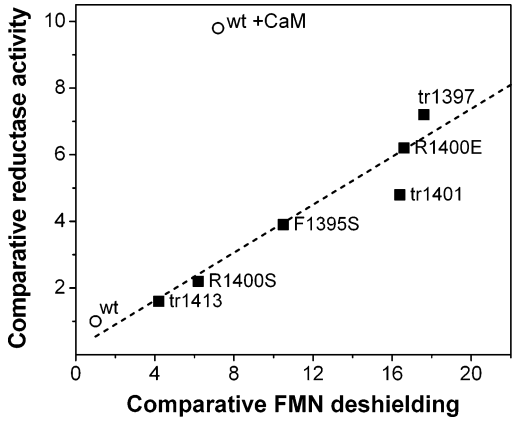

FIGURE 8: Correlation between the steady-state cytochrome *c* reductase activity and the degree of FMN deshielding for nNOSr proteins. The indicated values were obtained from this report or from ref 21 (R1400S, R1400E) or unpublished data (F1395S). The least-squares line of best fit is indicated.

Relationship between FMN Shielding and the Reductase Activity of nNOSr. NOSr and related flavoproteins are thought to exist in a conformational equilibrium between FMN-shielded and FMN-deshielded states that respectively enable electrons to enter into or exit from the FMN cofactor (*19*−*25*, *59*). Daff and colleagues (*19*) were the first to propose that an inverse relationship might exist between the degree of FMN shielding and the cytochrome *c* reductase activity of CaM-free nNOSr. This proposal was based on measures taken with nNOSr samples that had been poised at three different states in the FMN conformational equilibrium (NADPH-free and CaM-free; NADPH-bound and CaM-free; and CaM-bound). Subsequent measures with point mutants that have altered FMN shielding (R1400E, R1400S, or F1395S nNOSr) generally lend support to the concept (*20*, *21*). However, our current study with CT truncation mutants allows us to examine the relationship over a much wider range of FMN shielding states than previously possible. Figure 8 plots the cytochrome *c* reductase activities we have measured for various nNOSr proteins in the CaM-free, NADPH-bound state *versus* their degree of FMN deshielding relative to the NADPH-bound wild-type nNOSr, to which we assigned reductase activity and FMN shielding values of unity. A strong inverse correlation does exist ($R = 0.96$) between the reductase activity and degree of FMN shielding across the entire experimental range represented in Figure 8. Remarkably, the relationship appears to be relatively independent of the means we used to change the FMN conformational equilibrium (CT point mutations *versus* the various CT truncations). Overall, the data establish that an inverse correlation exists between FMN shielding and the cytochrome *c* reductase activity, and reveal that the CT determines the baseline or set point value for the FMN conformational equilibrium in CaM-free nNOSr.

CT and the CaM Response of nNOS. Our study helps address some questions about CaM's mechanism of action in NOS enzymes. First, does CaM relieve suppression of nNOSr by a mechanism that is dependent on or independent of the CT? Our data strongly support CT involvement because (i) the full CT deletion has effects nearly equivalent to CaM binding on many of the measured parameters (Tables 1 and 7), and (ii) CaM binding to CT-truncated nNOSr had very little additional impact. Thus, we conclude that CaM relieves suppression of nNOSr through an effect on CT function. But how is the effect of CaM binding transduced through nNOSr? One possible mechanism has CaM destabilizing an interaction between CT and the autoinhibitory insert (AI) in the FMN module in order to relieve suppression of nNOSr (*23*, *27*, *35*, *37*). Geometric constraints apparent in the crystal structure of nNOSr imply that the AI cannot directly interact with the CT α-helix (*17*). However, the AI could still conceivably interact with the terminal half of CT, which although invisible in the crystal structure can be imagined to extend a significant distance (as shown in Figure 7A). Despite this possibility, our data with the tr1413 nNOS enzymes show that the terminal half of CT is not required for any of the CaM responses that we measured. If the terminal half of CT was involved in the CaM response, then we would expect CaM to have been unable to impact multiple parameters in the tr1413 nNOS mutants. Thus, our data argue against models for CaM function that involve AI interaction with the terminal half of CT, and suggest that an alternative mechanism exists. Perhaps CaM enables the AI to interact with the CT α-helix despite the physical constraints apparent in the crystal structure, or perhaps CaM influences CT function by an entirely different means.

Does the FMN deshielding caused by CaM fully explain its ability to increase the cytochrome *c* reductase activity of nNOSr? Our data in Figure 8 suggest that it does not. Specifically, the CaM-free nNOSr proteins whose positions on the FMN shielding continuum are similar to CaM-bound nNOSr (i.e., those having an *x*-axis value near 8 in Figure 8) have reductase activities that are only about one-third that of CaM-bound nNOSr. In fact, the CT truncation mutants have to reach a level of FMN deshielding that is 2 to 3 times greater than that caused by CaM in order to approach the same reductase activity (Figure 8). It is unclear what other effects of CaM binding enable it to support a higher reductase activity at its particular level of FMN shielding. Possible effects include CaM-dependent changes in the flavin reduction rate (Table 3) (*39*) or in the flavin reduction potentials (*24*). Clearly, CaM regulation of reductase activity is multicomponent and should be further investigated.

Does the CT enable CaM to effect NOS heme reduction and NO synthesis? We found that CaM supported near-normal rates of heme reduction and NO synthesis in tr1401 nNOS, which means that the CT α-helix has little to do with these CaM responses. Indeed, an independence between CaM responses that are reductase-specific (FMN shielding, cytochrome *c* reductase activity) and CaM responses that involve electron transfer between the NOS reductase and oxygenase domains (heme reduction, NO synthesis) has been previously described and discussed (*24*, *45*, *60*−*63*). The data presented show that the CT α-helix is primarily responsible for suppressing CaM responses in nNOS that are reductase-specific. However, this ultimately is an incomplete description of CT function, because point mutagenesis within the CT (at residues R1400 or S1412) increases the heme reduction rate in CaM-bound nNOS (*21*, *38*). But the mechanism in this case must involve some precise CT function, because truncating part or all of the CT did not increase heme reduction rate or NO synthesis in any case, and instead caused these parameters to decrease (Table 6). Perhaps the increased heme reduction in the S1412D and R400E nNOS mutants is due to the introduction of a

repulsive charge in the CT whereas simple removal of CT interactions by truncation is insufficient.

Interestingly, the additional deletion of the four residues upstream from the CT α-helix (tr1397 nNOS) caused the heme reduction rate and NO synthesis activity to decrease by about 50% and also allowed some heme reduction and NO synthesis to occur in the CaM-free enzyme. Our work reveals that these effects are independent of the CT α-helix, and so may inherently differ from the other effects attributed to the CT in this study. The mechanism in this case may involve a direct effect of the four residues on the FNR module and deserves further investigation.

ACKNOWLEDGMENT

We thank Ms. Deborah Durra for excellent technical assistance and Dr. Mohammad Mahfuzul Haque and Dr. David W. Konas for helpful advice and discussions.

REFERENCES

1. Stuehr, D. J. (1999) Mammalian nitric oxide synthases, *Biochim. Biophys. Acta 1411*, 217−230.
2. Michel, T., and Feron, O. (1997) Nitric oxide synthases: which, where, how, and why?, *J. Clin. Invest. 100*, 2146−2152.
3. Ricciardolo, F. L., Sterk, P. J., Gaston, B., and Folkerts, G. (2004) Nitric oxide in health and disease of the respiratory system, *Physiol. Rev. 84*, 731−765.
4. Ignarro, L. J., and Napoli, C. (2005) Novel features of nitric oxide, endothelial nitric oxide synthase, and atherosclerosis, *Curr. Diabetes Rep. 5*, 17−23.
5. Moncada, S. (1999) Nitric oxide: discovery and impact on clinical medicine, *J. R. Soc. Med. 92*, 164−169.
6. Alderton, W. K., Cooper, C. E., and Knowles, R. G. (2001) Nitric oxide synthases: structure, function and inhibition, *Biochem. J. 357*, 593−615.
7. Li, H., and Poulos, T. L. (2005) Structure-function studies on nitric oxide synthases, *J. Inorg. Biochem. 99*, 293−305.
8. Wei, C. C., Crane, B. R., and Stuehr, D. J. (2003) Tetrahydrobiopterin radical enzymology, *Chem. Rev. 103*, 2365−2383.
9. Hurshman, A. R., and Marletta, M. A. (2002) Reactions catalyzed by the heme domain of inducible nitric oxide synthase: evidence for the involvement of tetrahydrobiopterin in electron transfer, *Biochemistry 41*, 3439−3456.
10. Bredt, D. S., Hwang, P. M., Glatt, C. E., Lowenstein, C., Reed, R. R., and Snyder, S. H. (1991) Cloned and expressed nitric oxide synthase structurally resembles cytochrome P-450 reductase, *Nature 351*, 714−718.
11. Masters, B., McMillan, K., Sheta, E., Nishimura, J., Roman, L., and Martasek, P. (1996) Neuronal nitric oxide synthase, a modular enzyme formed by convergent evolution: structure studies of a cysteine thiolate-liganded heme protein that hydroxylates L-arginine to produce NO. as a cellular signal, *FASEB J. 10*, 552−558.
12. Wang, M., Roberts, D. L., Paschke, R., Shea, T. M., Masters, B. S., and Kim, J. J. (1997) Three-dimensional structure of NADPH-cytochrome P450 reductase: prototype for FMN- and FAD-containing enzymes, *Proc. Natl. Acad. Sci. U.S.A. 94*, 8411−8416.
13. Zhang, J., Martasek, P., Paschke, R., Shea, T., Siler Masters, B. S., and Kim, J. J. (2001) Crystal structure of the FAD/NADPH-binding domain of rat neuronal nitric-oxide synthase. Comparisons with NADPH-cytochrome P450 oxidoreductase, *J. Biol. Chem. 276*, 37506−37513.
14. Matsuda, H., and Iyanagi, T. (1999) Calmodulin activates intramolecular electron transfer between the two flavins of neuronal nitric oxide synthase flavin domain, *Biochim. Biophys. Acta 1473*, 345−355.
15. Daff, S., Noble, M. A., Craig, D. H., Rivers, S. L., Chapman, S. K., Munro, A. W., Fujiwara, S., Rozhkova, E., Sagami, I., and Shimizu, T. (2001) Control of electron transfer in neuronal NO synthase, *Biochem. Soc. Trans. 29*, 147−152.
16. Garnaud, P. E., Koetsier, M., Ost, T. W., and Daff, S. (2004) Redox properties of the isolated flavin mononucleotide- and flavin adenine dinucleotide-binding domains of neuronal nitric oxide synthase, *Biochemistry 43*, 11035−11044.
17. Garcin, E. D., Bruns, C. M., Lloyd, S. J., Hosfield, D. J., Tiso, M., Gachhui, R., Stuehr, D. J., Tainer, J. A., and Getzoff, E. D. (2004) Structural basis for isozyme-specific regulation of electron transfer in nitric-oxide synthase, *J. Biol. Chem. 279*, 37918−37927.
18. Ludwig, M. L., and Marletta, M. A. (1999) A new decoration for nitric oxide synthase−a Zn(Cys)4 site, *Structure 7*, R73−R79.
19. Craig, D. H., Chapman, S. K., and Daff, S. (2002) Calmodulin activates electron transfer through neuronal nitric-oxide synthase reductase domain by releasing an NADPH-dependent conformational lock, *J. Biol. Chem. 277*, 33987−33994.
20. Konas, D. W., Zhu, K., Sharma, M., Aulak, K. S., Brudvig, G. W., and Stuehr, D. J. (2004) The FAD-shielding residue Phe1395 regulates neuronal nitric-oxide synthase catalysis by controlling NADP+ affinity and a conformational equilibrium within the flavoprotein domain, *J. Biol. Chem. 279*, 35412−35425.
21. Tiso, M., Konas, D. W., Panda, K., Garcin, E. D., Sharma, M., Getzoff, E. D., and Stuehr, D. J. (2005) C-terminal tail residue Arg1400 enables NADPH to regulate electron transfer in neuronal nitric-oxide synthase, *J. Biol. Chem. 280*, 39208−39219.
22. Panda, K., Haque, M. M., Garcin-Hosfield, E. D., Durra, D., Getzoff, E. D., and Stuehr, D. J. (2006) Surface charge interactions of the FMN module govern catalysis by nitric-oxide synthase, *J. Biol. Chem. 281*, 36819−36827.
23. Roman, L., and Masters, B. (2006) Electron transfer by neuronal nitric-oxide synthase is regulated by concerted interaction of calmodulin and two intrinsic regulatory elements, *J. Biol. Chem. 281*, 23111−23118.
24. Dunford, A., Rigby, S., Hay, S., Munro, A., and Scrutton, N. (2007) Conformational and Thermodynamic Control of Electron Transfer in Neuronal Nitric Oxide Synthase, *Biochemistry 46*, 5018−5029.
25. Grunau, A., Paine, M. J., Ladbury, J. E., and Gutierrez, A. (2006) Global effects of the energetics of coenzyme binding: NADPH controls the protein interaction properties of human cytochrome P450 reductase, *Biochemistry 45*, 1421−1434.
26. Abu-Soud, H. M., and Stuehr, D. J. (1993) Nitric oxide synthases reveal a role for calmodulin in controlling electron transfer, *Proc. Natl. Acad. Sci. U.S.A. 90*, 10769−10772.
27. Salerno, J. C., Harris, D. E., Irizarry, K., Patel, B., Morales, A. J., Smith, S. M., Martasek, P., Roman, L. J., Masters, B. S., Jones, C. L., Weissman, B. A., Lane, P., Liu, Q., and Gross, S. S. (1997) An autoinhibitory control element defines calcium-regulated isoforms of nitric oxide synthase, *J. Biol. Chem. 272*, 29769−29777.
28. Daff, S., Sagami, I., and Shimizu, T. (1999) The 42-amino acid insert in the FMN domain of neuronal nitric-oxide synthase exerts control over Ca(2+)/calmodulin-dependent electron transfer, *J. Biol. Chem. 274*, 30589−30595.
29. Montgomery, H. J., Romanov, V., and Guillemette, J. G. (2000) Removal of a putative inhibitory element reduces the calcium-dependent calmodulin activation of neuronal nitric-oxide synthase, *J. Biol. Chem. 275*, 5052−5058.
30. Chen, P. F., and Wu, K. K. (2000) Characterization of the roles of the 594−645 region in human endothelial nitric-oxide synthase in regulating calmodulin binding and electron transfer, *J. Biol. Chem. 275*, 13155−13163.
31. Knudsen, G. M., Nishida, C. R., Mooney, S. D., and Ortiz, de Montellano, P. R. (2003) Nitric-oxide synthase (NOS) reductase domain models suggest a new control element in endothelial NOS that attenuates calmodulin-dependent activity, *J. Biol. Chem. 278*, 31814−31824.
32. Roman, L. J., Martasek, P., Miller, R. T., Harris, D. E., de La, Garza, M. A., Shea, T. M., Kim, J. J., and Masters, B. S. (2000) The C termini of constitutive nitric-oxide synthases control electron flow through the flavin and heme domains and affect modulation by calmodulin, *J. Biol. Chem. 275*, 29225−29232.
33. Roman, L. J., Miller, R. T., de La, Garza, M. A., Kim, J. J., and Siler, Masters, B. S. (2000) The C terminus of mouse macrophage inducible nitric-oxide synthase attenuates electron flow through the flavin domain, *J. Biol. Chem. 275*, 21914−21919.
34. Nishida, C. R., and de Montellano, P. R. (2001) Control of electron transfer in nitric-oxide synthases. Swapping of autoinhibitory elements among nitric-oxide synthase isoforms, *J. Biol. Chem. 276*, 20116−20124.
35. Lane, P., and Gross, S. S. (2002) Disabling a C-terminal autoinhibitory control element in endothelial nitric-oxide synthase by phosphorylation provides a molecular explanation for activation

of vascular NO synthesis by diverse physiological stimuli, *J. Biol. Chem. 277*, 19087−19094.
36. Rozhkova, E., Fujimoto, N., Sagami, I., Daff, S., and Shimizu, T. (2002) Interactions between the isolated oxygenase and reductase domains of neuronal nitric-oxide synthase: assessing the role of calmodulin, *J. Biol. Chem. 277*, 16888−16894.
37. Chen, P. F., and Wu, K. K. (2003) Structural elements contribute to the calcium/calmodulin dependence on enzyme activation in human endothelial nitric-oxide synthase, *J. Biol. Chem. 278*, 52392−52400.
38. Adak, S., Santolini, J., Tikunova, S., Wang, Q., Johnson, J. D., and Stuehr, D. J. (2001) Neuronal nitric-oxide synthase mutant (Ser-1412 → Asp) demonstrates surprising connections between heme reduction, NO complex formation, and catalysis, *J. Biol. Chem. 276*, 1244−1252.
39. Siddhanta, U., Wu, C., Abu-Soud, H. M., Zhang, J., Ghosh, D. K., and Stuehr, D. J. (1996) Heme iron reduction and catalysis by a nitric oxide synthase heterodimer containing one reductase and two oxygenase domains, *J. Biol. Chem. 271*, 7309−7312.
40. Gachhui, R., Ghosh, D. K., Wu, C., Parkinson, J., Crane, B. R., and Stuehr, D. J. (1997) Mutagenesis of acidic residues in the oxygenase domain of inducible nitric-oxide synthase identifies a glutamate involved in arginine binding, *Biochemistry 36*, 5097−5103.
41. Wei, C. C., Wang, Z. Q., and Stuehr, D. J. (2002) Nitric oxide synthase: use of stopped-flow spectroscopy and rapid-quench methods in single-turnover conditions to examine formation and reactions of heme-O2 intermediate in early catalysis, *Methods Enzymol. 354*, 320−338.
42. Wu, C., Zhang, J., Abu-Soud, H., Ghosh, D. K., and Stuehr, D. J. (1996) High-level expression of mouse inducible nitric oxide synthase in *Escherichia coli* requires coexpression with calmodulin, *Biochem. Biophys. Res. Commun. 222*, 439−444.
43. Stuehr, D. J., and Ikeda-Saito, M. (1992) Spectral characterization of brain and macrophage nitric oxide synthases. Cytochrome P-450-like hemeproteins that contain a flavin semiquinone radical, *J. Biol. Chem. 267*, 20547−20550.
44. Adak, S., Ghosh, S., Abu-Soud, H. M., and Stuehr, D. J. (1999) Role of reductase domain cluster 1 acidic residues in neuronal nitric-oxide synthase. Characterization of the FMN-FREE enzyme, *J. Biol. Chem. 274*, 22313−22320.
45. Knight, K., and Scrutton, N. S. (2002) Stopped-flow kinetic studies of electron transfer in the reductase domain of neuronal nitric oxide synthase: re-evaluation of the kinetic mechanism reveals new enzyme intermediates and variation with cytochrome P450 reductase, *Biochem. J. 367*, 19−30.
46. Schwede, T., Kopp, J., Guex, N., and Peitsch, M. C. (2003) SWISS-MODEL: An automated protein homology-modeling server, *Nucleic Acids Res. 31*, 3381−3385.
47. Guex, N., and Peitsch, M. C. (1997) SWISS-MODEL and the Swiss-PdbViewer: an environment for comparative protein modeling, *Electrophoresis 18*, 2714−2723.
48. Laskowski, R. A., MacArthur, M. W., Moss, D. S., and Thornton, J. M. (1993) PROCHECK: a program to check the stereochemical quality of protein structures, *J. Appl. Crystallogr. 26*, 283−291.
49. Hubbard, P. A., Shen, A. L., Paschke, R., Kasper, C. B., and Kim, J. J. (2001) NADPH-cytochrome P450 oxidoreductase. Structural basis for hydride and electron transfer, *J. Biol. Chem. 276*, 29163−29170.
50. Adak, S., Sharma, M., Meade, A. L., and Stuehr, D. J. (2002) A conserved flavin-shielding residue regulates NO synthase electron transfer and nicotinamide coenzyme specificity, *Proc. Natl. Acad. Sci. U.S.A. 99*, 13516−13521.
51. Dunford, A. J., Marshall, K. R., Munro, A. W., and Scrutton, N. S. (2004) Thermodynamic and kinetic analysis of the isolated FAD domain of rat neuronal nitric oxide synthase altered in the region of the FAD shielding residue Phe1395, *Eur. J. Biochem. 271*, 2548−2560.
52. Deng, Z., Aliverti, A., Zanetti, G., Arakaki, A. K., Ottado, J., Orellano, E. G., Calcaterra, N. B., Ceccarelli, E. A., Carrillo, N., and Karplus, P. A. (1999) A productive NADP+ binding mode of ferredoxin-NADP + reductase revealed by protein engineering and crystallographic studies, *Nat. Struct. Biol. 6*, 847−853.
53. Tejero, J., Perez-Dorado, I., Maya, C., Martinez-Julvez, M., Sanz-Aparicio, J., Gomez-Moreno, C., Hermoso, J. A., and Medina, M. (2005) C-terminal tyrosine of ferredoxin-NADP+ reductase in hydride transfer processes with NAD(P)+/H, *Biochemistry 44*, 13477−13490.
54. Piubelli, L., Aliverti, A., Arakaki, A., Carrillo, N., Ceccarelli, E., Karplus, P., and Zanetti, G. (2000) Competition between C-terminal tyrosine and nicotinamide modulates pyridine nucleotide affinity and specificity in plant ferredoxin-NADP(+) reductase, *J. Biol. Chem. 275*, 10472−10476.
55. Abu-Soud, H. M., Yoho, L. L., and Stuehr, D. J. (1994) Calmodulin controls neuronal nitric-oxide synthase by a dual mechanism. Activation of intra- and interdomain electron transfer, *J. Biol. Chem. 269*, 32047−32050.
56. Panda, K., Adak, S., Konas, D., Sharma, M., and Stuehr, D. J. (2004) A conserved aspartate (Asp-1393) regulates NADPH reduction of neuronal nitric-oxide synthase: implications for catalysis, *J. Biol. Chem. 279*, 18323−18333.
57. Gachhui, R., Presta, A., Bentley, D. F., Abu-Soud, H. M., McArthur, R., Brudvig, G., Ghosh, D. K., and Stuehr, D. J. (1996) Characterization of the reductase domain of rat neuronal nitric oxide synthase generated in the methylotrophic yeast *Pichia pastoris*. Calmodulin response is complete within the reductase domain itself, *J. Biol. Chem. 271*, 20594−20602.
58. Noble, M. A., Munro, A. W., Rivers, S. L., Robledo, L., Daff, S. N., Yellowlees, L. J., Shimizu, T., Sagami, I., Guillemette, J. G., and Chapman, S. K. (1999) Potentiometric analysis of the flavin cofactors of neuronal nitric oxide synthase, *Biochemistry 38*, 16413−16418.
59. Grunau, A., Geraki, K., Grossmann, J. G., and Gutierrez, A. (2007) Conformational dynamics and the energetics of protein−ligand interactions: role of interdomain loop in human cytochrome P450 reductase, *Biochemistry 46*, 8244−8255.
60. Feng, C., Tollin, G., Holliday, M. A., Thomas, C., Salerno, J. C., Enemark, J. H., and Ghosh, D. K. (2006) Intraprotein electron transfer in a two-domain construct of neuronal nitric oxide synthase: the output state in nitric oxide formation, *Biochemistry 45*, 6354−6362.
61. Newman, E., Spratt, D. E., Mosher, J., Cheyne, B., Montgomery, H. J., Wilson, D. L., Weinberg, J. B., Smith, S. M., Salerno, J. C., Ghosh, D. K., and Guillemette, J. G. (2004) Differential activation of nitric-oxide synthase isozymes by calmodulin-troponin C chimeras, *J. Biol. Chem. 279*, 33547−33557.
62. Gachhui, R., Abu-Soud, H. M., Ghosha, D. K., Presta, A., Blazing, M. A., Mayer, B., George, S. E., and Stuehr, D. J. (1998) Neuronal nitric-oxide synthase interaction with calmodulin-troponin C chimeras, *J. Biol. Chem. 273*, 5451−5454.
63. Stevens-Truss, R., Beckingham, K., and Marletta, M. A. (1997) Calcium binding sites of calmodulin and electron transfer by neuronal nitric oxide synthase, *Biochemistry 36*, 12337−12345.

BI701646K